Supporting Information

Hettmer et al. 10.1073/pnas.1111733108

SI Materials and Methods

Myogenic Differentiation Assays. Freshly sorted cells were plated at 1×10^4 cells per well in 96-well plates coated with 1 μg/mL rat-tail collagen (Sigma) and 10 μg/mL natural mouse laminin (Invitrogen). Cells were expanded for 5–7 d in growth medium composed of Ham's F-10, 20% (vol/vol) horse serum, 1% penicillin/streptomycin, and 5 ng/mL basic Fibroblast growth factor (bFGF) (Sigma). bFGF was replaced daily. After 5–7 d, cells were passaged by aspiration of medium. Cells were replated onto chamber slides coated with 0.2% Matrigel (Fisher) in growth medium for 2 d; then medium was changed to differentiation medium consisting of Ham's F-10, 2% (vol/vol) horse serum, and 1% (vol/vol) penicillin/streptomycin. Cells were kept in differentiation medium for 6 d; then medium was aspirated, and cells were fixed with 4% (vol/vol) paraformaldehyde and processed for immunofluorescence (1).

Adipogenic Differentiation Assay. Freshly sorted cells were expanded as described above. After 5–7 d, cells were replated onto 0.2% (vol/vol) Matrigel-coated 48-well plates in growth medium for 2 d. Subsequently, medium was changed to adipogenic induction medium consisting of DMEM, 10% (vol/vol) FBS, 1% (vol/vol) penicillin/streptomycin, 1 mM dexamethasone (Sigma), 100 nM insulin (Sigma), 1 mM roziglitazone (Cayman Chemical), and 0.5 mM 3-isobutyl-1-methylxanthine (Sigma) for 2 d. Medium then was replaced with adipogenic differentiation medium consisting of DMEM, 10% (vol/vol) FBS, 1% (vol/vol) penicillin/streptomycin, and 100 nM insulin. Cells were kept in this medium for 6 d; then medium was aspirated, and cells were fixed with 4% (vol/vol) paraformaldehyde and stained with Oil-Red-O (Sigma) for 1 h at room temperature (2). Oil-Red-O staining of lipid droplets within adipocytes was analyzed by standard microscopy using an Olympus IX51 inverted microscope.

Preparation of Lentiviral Vectors. The 293T cell line was used for transient lentiviral vector production. The *Kras*(*G12V*)-IRES-GFP pGIPZ plasmid (15 μg) or pGIPZ vector plasmid (15 μg), the HIV gag-pol-REV expression plasmid pCMV-dR8.91 (9.75 μg), and the envelope expression plasmid pMD2.VSV.G (5.75 μg) were cotransfected into 293T cells, and lentivirus-containing supernatant was concentrated by ultracentrifugation at 19,500 rpm (Beckman L7 ultracentrifuge) for 3 h at 4 °C. Lentivirus was kept at −80 °C for ≤ 3 wk.

Lentiviral Transduction of Myofiber-Associated Cells. Lentivirus titers were determined by transduction of 293T cells and measurement of the percent GFP^+ cells by flow cytometry after 3 d. Freshly isolated subsets of myofiber-associated cells (MFA) were plated in growth medium composed of Ham's F-10, 20% (vol/vol) horse serum, 1% (vol/vol) penicillin/streptomycin, and 5 ng/mL bFGF (Sigma) at 1×10^4 cells per well in 96-well plates coated with 1 μg/mL rat-tail collagen and 10 μg/mL natural mouse laminin. Within 1–2 h after sorting, 8 μg/mL polyprene and lentivirus (multiplicity of infection of 0.5–1) were added and incubated for 24 h. Medium then was replaced with fresh growth medium for an additional 12–24 h before transplantation.

Sarcoma-Induction Strategy. The sarcoma-induction strategy described here was designed to evaluate prospectively the impact of cell context on tumor-specific phenotype following the introduction of identical oncogenetic lesions into distinct cell populations (with distinct lineage and differentiation potentials) that reside in the same anatomical location. Specifically, sarcomas were induced by ectopic expression of *Kras*(*G12V*) and inactivation of the *CDKN2A* gene locus in three distinct muscle-resident cell populations isolated by direct cell sorting, including two cell populations for which appropriate lineage-specific Cre drivers are unavailable [i.e., $CD45^-MAC1^-TER119^-Sca1^+$ and $CD45^-MAC1^-TER119^-Sca1^-CXCR4^-$ cells]. Using the lentiviral strategy, we were able to deliver roughly equivalent "doses" of activated *Kras* (Fig. S2) and concomitantly mark the cells in which oncogenic *Kras* was expressed by virally encoded GFP.

Mouse Tumor Immunohistochemistry. For immunohistochemistry, 4-μm sections of paraffin-embedded tissue were baked, deparaffinized, and subjected to heat-induced antigen retrieval in target retrieval solution, pH9 (Dako). Sections then were treated with peroxidase and protein blockers (Dako) and incubated with antibodies against myogenin (1:100; M3559; Dako,), MyoD1 (1:50; M3512; Dako), desmin (1:50; M0760; Dako), phosphorylated ERK (p-ERK) (1:200; 4370; Cell Signaling Technonogy), and phosphorylated S6 (p-S6) (1:200; 4060, Cell Signaling Technonogy) at room temperature for 1 h. The detection system was mouse Envision (Dako) for 30 min followed by development with a 3,3V-diaminobenzidine chromagen substrate for 5 min. For GFP staining, 4-μm sections of paraffin-embedded tissue were subjected to heat-induced antigen retrieval in AR Vector solution (Vector Laboratories) and were incubated overnight with antibody against GFP (1:1,500; 632381; Clontech) at 4 °C. Biotinylated secondary antibody was incubated for 30 min. The tertiary detection system was Vectastain ABC (Vector Laboratories) with a 3,3V-diaminobenzidine chromagen substrate. Slides were lightly counterstained with hematoxylin. Isotype-specific antibodies were used as negative controls.

Human Tissue Arrays. Tissue arrays were purchased from US Biomax (S02081, human smooth muscle and striated muscle cancer progression). Each array included 58 leiomyosarcoma cores, 48 rhabdomyosarcoma (RMS) cores, 16 striated muscle tissue cores and 10 smooth muscle cores, representing 29 leiomyosarcomas, 24 RMS cases, eight striated muscle specimens, and five smooth muscle specimens (in duplicates). Two leiomyosarcoma cases were excluded because of poor core quality. One RMS case was excluded from evaluation for p-S6 because of poor core quality. Staining was graded by two independent operators.

FACS Antibody Staining. For FACS sorting of normal MFA cells, the following primary and secondary antibodies were used: phycoerythrin (PE)-conjugated anti-mouse TER119 (1:200; 12–5921-82; eBioscience), PE-conjugated anti-mouse CD11b (1:200; 12–0112-82; eBioscience), PE-conjugated anti-mouse CD45 (1:200; 12–0451-83; eBioscience), allophycocyanin-conjugated anti-mouse Sca1 (1:200; 17–5981-82; eBioscience), purified Armenian hamster anti-mouse CD29 (1:200; 553837; BD Pharmingen), biotin rat anti-mouse CD184 (1:100; 551968; BD Pharmingen), Phycoerythrin-Cy-7 (PECY7)-conjugated streptavidin (1:200; 25–4317-82; eBioscience), and Fluorescein isothiocyanate (FITC)-conjugated anti-Armenian hamster IgG (1:200; 11–4111-85; eBioscience). Antibody staining was performed for 20 min on ice.

RT -PCR. Tumor samples were FACS sorted to isolate GFP^+ cells. mRNA was isolated by TRIzol extraction and reverse transcribed using SuperScript III First-Strand Synthesis System for RT-PCR (Invitrogen). Quantitative RT-PCR (qRT-PCR) was

performed using an AV7900 PCR system (Applied Biosystems) with SYBR-green PCR reagents. MyoD and myogenin were detected using the following primer sequences: MyoD, forward, 5′-TGG-TTC-TTC-ACG-CCC-AAA-AG-3′ and MyoD reverse, 5′-TCT-GGA-AGA-ACG-GCT-TCG-AA-3′; myogenin forward, 5′-CTA-CAG-GCC-TTG-CTC-AGC-TC-3′ and myogenin reverse, 5′-TGT-GCG-AGT-TGC-ATT-CAC-TG-3′. *Kras* was detected with the primers: *Kras* forward, 5′-GAG-TAC-AGT-GCA-ATG-AGG-GAC-3′ and *Kras* reverse, 5′-CCT-GAG-CCT-GTT-TTG-TGT-CTA-C-3′. RT-PCR data were quantified using the standard curve method, and relative expression of MyoD and myogenin per sample was determined by normalization against the quantity of 18s rRNA within each sample. For each sample, qRT-PCR was performed in technical triplicates, and results were averaged.

Immunofluorescence Analysis. Immunofluorescence was performed on paraformaldehyde-fixed MFA cells grown in chamber slides. Cells were permeabilized with 0.2% (vol/vol) Triton X-100 and blocked before staining using the M.O.M. blocking kit (Vector Labs) and 10% (vol/vol) goat serum. Sections were stained with primary antibody (monoclonal anti-myosin antibody, clones MY-31 and NOQ7.5.4D; 1:50 each; Sigma) at 4 °C overnight and with secondary antibody (goat anti-mouse-594 conjugate; 1:200; Invitrogen) for 1 h at room temperature. The GFP signal was amplified using anti–GFP-488 (1:200; Invitrogen) conjugate. Slides were coverslipped using Vectashield mounting medium with DAPI to stain nuclei. Immunofluorescent labeling was analyzed by standard fluorescence microscopy using an Olympus BX60 upright microscope.

Microarray Analysis. CEL files were imported into dChip (Cheng Li laboratory, Dana-Farber Cancer Institute, Boston, MA), along with published CEL files representing normal mouse skeletal muscle (3–6). Samples were normalized in batch against an invariant set. Filtered probe sets were identified based on variation across samples being $1 < \text{SD/mean} < 1{,}000$ with 50% of probes being present in array comparisons. Expression level cut-offs were made at >600, >400, and >200 with expression being found in ≥50% of microarray samples. In this analysis, 242, 406, and 829 differentially regulated probe sets were identified and used for hierarchical clustering. Tumor samples reproducibly failed to cluster based on cell-of-origin, independent of the filtered probe list used.

Comparisons between tumor samples and normal skeletal muscle (the anatomic site from which tumor cells-of-origin were isolated and where tumors emerged) were made in dChip. Differentially regulated gene sets were identified based on the following criteria: Baseline/Experiment (B/E) or Experiment/Baseline (E/B) (fold-change) >10 using a 90% confidence bound of fold-change, E/B or B/E >2, P value for testing $E = B < 0.05$, and percent call of B ≥20% or E ≥20%. To account for multiple comparisons, 50 permutations of the data were completed. From this analysis, 1,116 differentially regulated probe sets were obtained that distinguish tumor from skeletal muscle with a median false-discovery rate (FDR) of 0% and the 90% FDR of 0%. Subsequently, various lists of up-regulated gene were generated based on fold-change differences between tumor and muscle. Log-scale transformation was not used because it biases P values and excludes underexpressed genes that are significantly regulated. Log-transformed data yielded results similar to those compiled using non–log-transformed data. Annotation of probe sets was completed using the Affymetrix NetAffx Analysis Center (http://www.affymetrix.com/analysis/index.affx).

For published microarray data sets (described in more detail in Dataset S1), original CEL files or GCT files were obtained (3-17). CEL files were imported into dChip and were normalized against an invariant set, and GCT files containing all probes were generated as previously described (18). Gene set enrichment analysis (GSEA) analysis was completed using phenotype permutation with a weighted enrichment statistic and a signal-to-noise metric for ranking genes. One thousand permutations of the data were completed to obtain an FDR q value. Significance was defined as having an FDR q value < 0.25 and a family-wise error rate (FWER) P value < 0.05. NetAffx was used to map genes across platforms using gene IDs. Gene ontology analyses of sarcoma signature genes were performed using Ingenuity (Ingenuity Systems Inc.).

Statistics. Sarcoma cell-of-origin frequencies were compared using likelihood ratio tests. Mean (± SD) MFA cell numbers and frequencies and skeletal muscle weight in $p16p19^{null}$ mice versus wild-type C57BL6 mice were calculated and tested for significant differences by Bonferroni's multiple comparison test. Also, mean (± SD) of cell frequencies within the GFP^+ fraction of all three primary sarcoma types and mean differences (± SD) in MTT uptake in sarcoma cell lines exposed to chemicals versus controls were calculated and tested for significant differences by Bonferroni's multiple comparison test. Time until palpability of primary tumors and time until death were evaluated by Kaplan–Meier analyses. Differences in expression of *Kras*, MyoD, and myogenin by tumor, skeletal muscle, and spleen cells were assessed by Bonferroni's multiple comparison test. Differences were considered statistically significant at $P < 0.05$.

1. Cerletti M, et al. (2008) Highly efficient, functional engraftment of skeletal muscle stem cells in dystrophic muscles. *Cell* 134(1):37–47.
2. Jing E, Gesta S, Kahn CR (2007) SIRT2 regulates adipocyte differentiation through FoxO1 acetylation/deacetylation. *Cell Metab* 6(2):105–114.
3. Haldar M, Hancock JD, Coffin CM, Lessnick SL, Capecchi MR (2007) A conditional mouse model of synovial sarcoma: Insights into a myogenic origin. *Cancer Cell* 11(4): 375–388.
4. Haldar, et al. (2009) A CreER-based random induction strategy for modeling translocation-associated sarcomas in mice. *Cancer Res* 69(8):3657–3664.
5. Mito JK, et al. (2009) Cross species genomic analysis identifies a mouse model as undifferentiated pleomorphic sarcoma/malignant fibrous histiocytoma. *PLoS ONE* 4 (11):e8075.
6. Nishijo K, et al. (2009) Credentialing a preclinical mouse model of alveolar rhabdomyosarcoma. *Cancer Res* 69(7):2902–2911.
7. Davicioni E, et al. (2009) Molecular classification of rhabdomyosarcoma—genotypic and phenotypic determinants of diagnosis: A report from the Children's Oncology Group. *Am J Pathol* 174(2):550–564.
8. Bild AH, et al. (2006) Oncogenic pathway signatures in human cancers as a guide to targeted therapies. *Nature* 439(7074):353–357.
9. Thorrez L, et al. (2008) Using ribosomal protein genes as reference: A tale of caution. *PLoS One* 3(3):e1854.
10. Chang JT, et al. (2009) A genomic strategy to elucidate modules of oncogenic pathway signaling networks. *Mol Cell* 34(1):104–114.
11. Hoeflich KP, et al. (2009) In vivo antitumor activity of MEK and phosphatidylinositol 3-kinase inhibitors in basal-like breast cancer models. *Clin Cancer Res* 15(14):4649–4664.
12. Kang PB, et al. (2005) Variations in gene expression among different types of human skeletal muscle. *Muscle Nerve* 32(4):483–491.
13. Landis MD, et al. (2005) Gene expression profiling of cancer progression reveals intrinsic regulation of transforming growth factor-beta signaling in ErbB2/Neu-induced tumors from transgenic mice. *Oncogene* 24(33):5173–5190.
14. Nakayama R, et al. (2007) Gene expression analysis of soft tissue sarcomas: Characterization and reclassification of malignant fibrous histiocytoma. *Mod Pathol* 20(7):749–759.
15. Oliver TG, et al. (2005) Loss of patched and disruption of granule cell development in a pre-neoplastic stage of medulloblastoma. *Development* 132(10):2425–2439.
16. Ramaswamy S, et al. (2001) Multiclass cancer diagnosis using tumor gene expression signatures. *Proc Natl Acad Sci USA* 98(26):15149–15154.
17. Zhou Y, et al. (2010) Chimeric mouse tumor models reveal differences in pathway activation between ERBB family- and KRAS-dependent lung adenocarcinomas. *Nat Biotechnol* 28(1):71–78.
18. Langenau DM, et al. (2007) Effects of RAS on the genesis of embryonal rhabdomyosarcoma. *Genes Dev* 21(11):1382–1395.

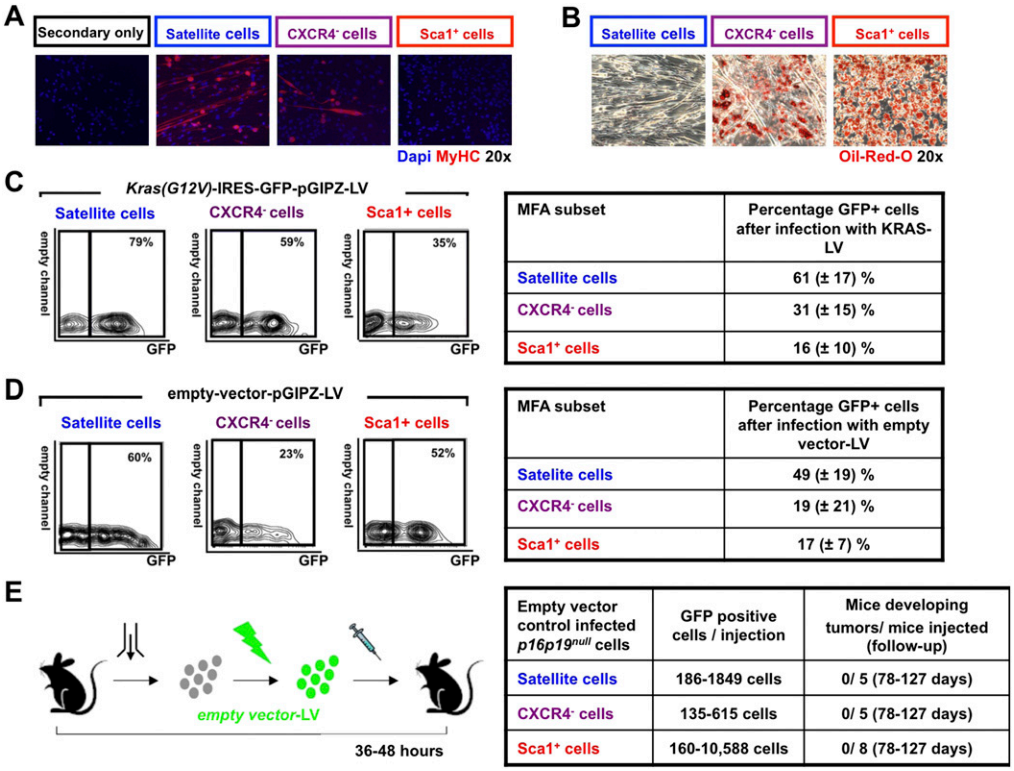

MFA subset	Percentage GFP+ cells after infection with KRAS-LV
Satellite cells	61 (± 17) %
CXCR4- cells	31 (± 15) %
Sca1+ cells	16 (± 10) %

MFA subset	Percentage GFP+ cells after infection with empty vector-LV
Satelite cells	49 (± 19) %
CXCR4- cells	19 (± 21) %
Sca1+ cells	17 (± 7) %

Empty vector control infected *p16p19null* cells	GFP positive cells / injection	Mice developing tumors/ mice injected (follow-up)
Satellite cells	186-1849 cells	0/ 5 (78-127 days)
CXCR4- cells	135-615 cells	0/ 5 (78-127 days)
Sca1+ cells	160-10,588 cells	0/ 8 (78-127 days)

Fig. S1. Functional properties of MFA cells isolated from skeletal muscle of *p16p19*^{null} mice, lentiviral transduction of mouse MFA cells, and lack of tumor formation by empty-vector pGIPZ lentivirus-infected MFA cells. (*A* and *B*) Loss of *p16p19* does not change the differentiation capacities of *p16p19*^{null} MFA cell subpopulations. (*A*) *p16p19*^{null} satellite cells and a subset of CXCR4^{-} cells give rise to myosin heavy chain-positive (MYHC^{+}) myoblasts and myofibers. (*B*) *p16p19*^{null} Sca1^{+} cells and a subset of CXCR4^{-} cells induce Oil-Red-O^{+} adipocytes. (*C* and *D*) Freshly isolated *p16p19*^{null} MFA cells were infected with *Kras*(*G12V*)-IRES-GFP pGIPZ lentivirus (*C*) or empty vector pGIPZ lentivirus (control) (*D*). Expression of GFP (mean ± SD) was evaluated by epifluorescence microscopy and flow cytometry 5–7 d after infection. Cells isolated from the CD45^{+}MAC1^{+}TER119^{+} fraction of MFA cells could not be maintained in standard growth medium, and consequently GFP positivity could not be evaluated in this subset of cells. (*E*) *p16p19*^{null} satellite cells, Sca1^{+} cells, and CXCR4^{-} cells were infected with empty-vector pGIPZ lentivirus and injected into the preinjured gastrocnemius muscles of NOD/SCID mice. Three independent experiments including a total of five to eight injections per cell population did not produce any tumors.

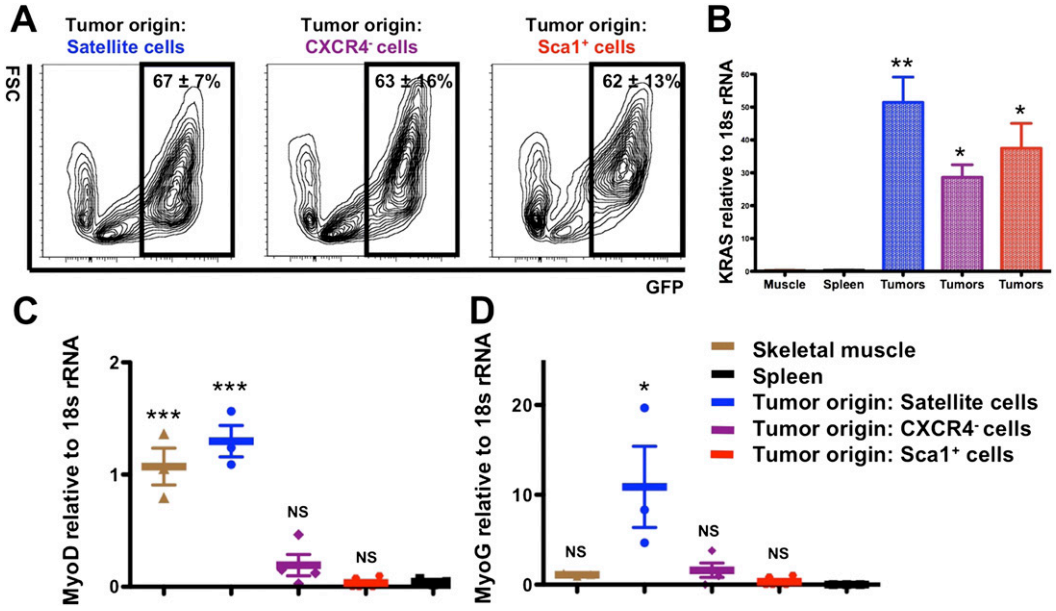

Fig. S2. *Kras* expression and differential expression of MyoD and myogenin in *Kras; p16p19^{null}* sarcomas. (*A*) Sarcomas arising from *Kras*(*G12V*)-expressing *p16p19^{null}* satellite cells, Sca1^{+} cells, and CXCR4^{-} cells contain 62–63% (± 7–16%) GFP^{+} cells (mean ± SD). (*B*) Expression of *Kras* was confirmed by qRT-PCR in GFP^{+} cells sorted from three tumors of satellite-cell origin, four tumors of Sca1^{+}-cell origin, and two tumors of CXCR4^{-}-cell origin and was compared with *p16p19^{null}* muscle or spleen cells (isolated from three mice). *Kras* expression was determined in triplicate and is presented as relative expression compared with 18s RNA (mean ± SD). Differences in *Kras* expression were evaluated by Bonferroni's multiple comparison test. (*C* and *D*) Expression of MyoD and myogenin was determined by qRT-PCR in GFP^{+} cells sorted from three tumors of satellite-cell origin, six tumors of Sca1^{+}-cell origin, and four tumors of CXCR4^{-}-cell origin and was compared with *p16p19^{null}* skeletal muscle and spleen cells (isolated from three mice). Expression of MyoD and myogenin was significantly higher in sarcomas of satellite cell-origin than in sarcomas of Sca1^{+}- or CXCR4^{-}-cell origin. As previously reported in the literature, myogenin expression in normal adult skeletal muscle is low (1). MyoD and myogenin expression were determined in triplicate and are presented as relative expression compared with 18s RNA (mean ± SD). Differences in MyoD and myogenin expression were evaluated by Bonferroni's multiple comparison test; NS, not significant; $*P < 0.5$; $**P < 0.1$; $***P < 0.001$ (compared with spleen samples).

1. Kumar S, Perlman E, Harris CA, Raffeld M, Tsokos M (2000) Myogenin is a specific marker for rhabdomyosarcoma: an immunohistochemical study in paraffin-embedded tissues. *Mod Pathol* 13(9):988–993.

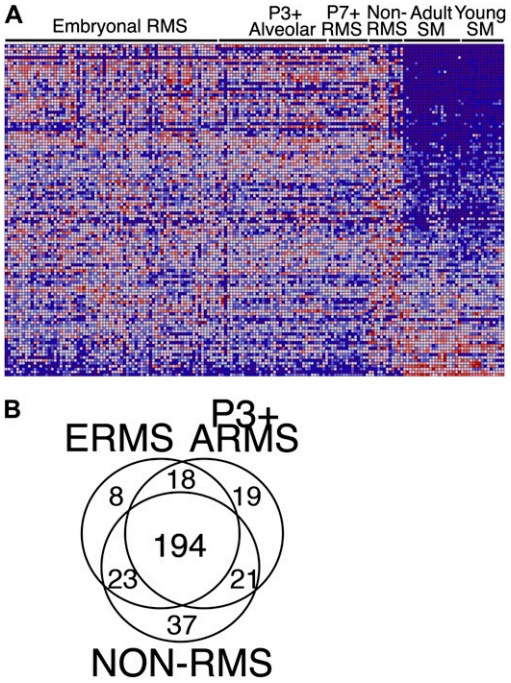

Fig. S3. Transcriptional profiling of *Kras; p16p19^{null}* mouse sarcomas. (*A*) Heatmap showing expression of genes upregulated in *Kras; p16p19^{null}* sarcomas across human RMS, non-RMS STS, and normal human skeletal muscle. See Dataset S2 for Gene IDs. (*B*) The upper quartile of genes, identified by GSEA analyses in Fig. 3 *A–C*, shows many overlapping genes, which are coordinately regulated in human RMS and non-RMS STS. The 194 overlapping probes (144 overlapping genes) obtained from *B* are listed in Table S3.

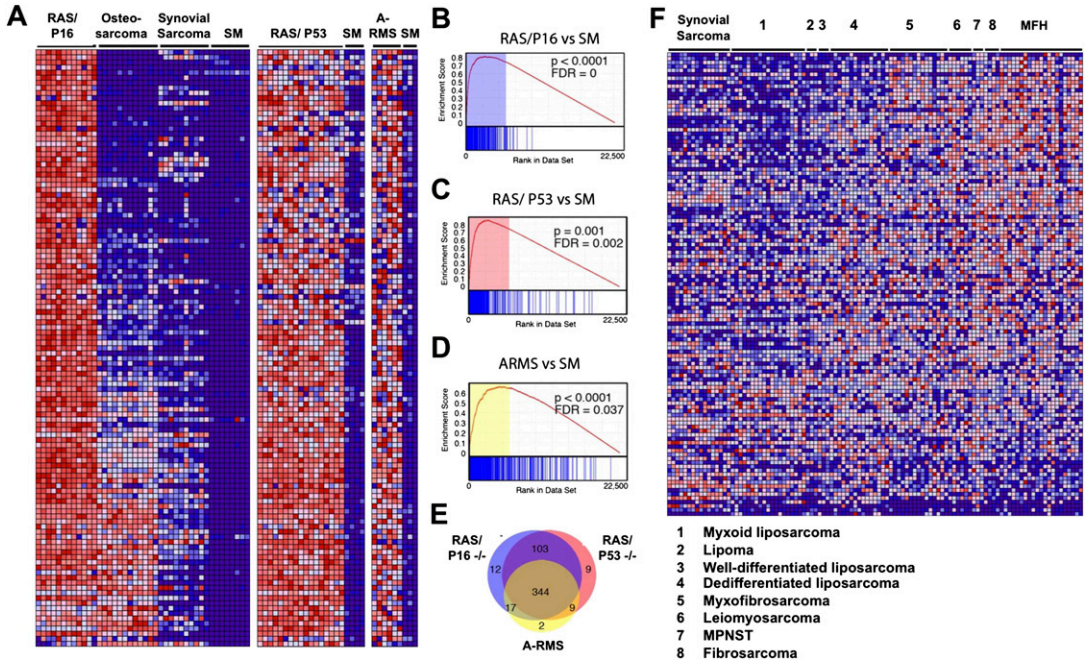

Fig. S4. Similarities in the transcriptional profile of *Kras; p16p19*^{null} mouse sarcomas, other mouse models of sarcoma, and human malignant fibrous histiocytoma (MFH). (*A*) Heatmap demonstrating expression of genes up-regulated >25-fold in mouse *Kras; p16p19*^{null} sarcomas compared with mouse skeletal muscle (SM) (gene IDs are listed in Dataset S3) across other mouse sarcoma models. There is a concordant increase in the expression of these genes in *Kras; Tp53*^{null} mouse sarcomas with myofibroblastic differentiation (KRAS/P53) and *PAX3-FKHR*$^{+}$*; TP53*^{null} mouse alveolar RMS (A-RMS). (*B–D*) Gene expression data also were evaluated by GSEA (details in Table S2) at up to four different fold-change cut-offs for (*B*) *Kras; p16p19*^{null} sarcomas ($P < 0.0001$, FDR = 0), (*C*) mouse *Kras;Tp53*$^{-/-}$ sarcomas ($P = 0.001$, FDR = 0.002) and (*D*) mouse alveolar rhabdomysarcoma ($P < 0.001$, FDR = 0.037) (*E*) The upper quartile of genes identified by GSEA analysis (marked in *B–D*) includes many overlapping genes that are coordinately up-regulated in *Kras; p16p19*^{null} sarcomas, *Kras; Tp53*^{null} mouse sarcomas with myofibroblastic differentiation, and *PAX3-FKHR*$^{+}$*; TP53*^{null} mouse alveolar RMS. (*F*) Heatmap demonstrating expression of genes up-regulated >25-fold in mouse *Kras; p16p19*^{null} sarcomas compared with mouse skeletal muscle (gene IDs listed in Dataset S4) across human sarcomas of adult age (18 synovial sarcomas, 3 well-differentiated liposarcomas, 15 dedifferentiated liposarcomas, 6 leiomyosarcomas, 3 fibrosarcomas, 21 malignant fibrous histiocytomas, 14 myxofibrosarcomas, 19 myxoid liposarcomas, 3 lipomas, and 3 malignant peripheral nerve sheath tumors (MPNST)). The *Kras; p16p19*^{null} sarcoma–up-regulated genes are highly expressed in malignant fibrous histiocytomas and, to a lesser degree, in other human sarcoma subtypes. GSEA at various fold-change levels also showed that *Kras; p16p19*^{null} sarcoma–up-regulated genes are enriched in malignant fibrous histiocytomas compared with other human sarcoma subtypes (details in Table S2).

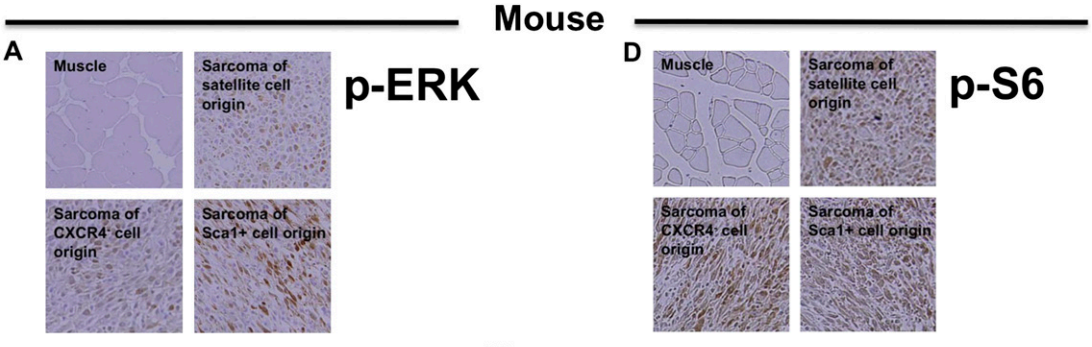

C

Tissue type (# biopsy cores evaluated)	Absent/ negligible p-ERK (# cores)	Positive p-ERK (# cores)	Reactivity for p-ERK (% cores)
Leiomyosarcoma (n = 27)	15	12	44%
Rhabdomyosarcoma (n = 24)	12	12	50%
Striated muscle (n = 8)	8	0	0%
Smooth muscle (n = 5)	3	2	40%

F

Tissue type (# biopsy cores evaluated)	Absent/ negligible p-S6 (# cores)	Positive p-S6 (# cores)	Reactivity for p-S6 (% cores)
Leiomyosarcoma (n = 27)	18	9	33%
Rhabdomyosarcoma (n = 23)	17	6	26%
Striated muscle (n = 8)	6	2	25%
Smooth muscle (n = 5)	2	3	60%

Fig. S5. Activation of Ras/Raf/MEK/ERK and mTOR signaling in sarcomas. (*A* and *D*) Mouse *Kras; p16p19^{null}* sarcomas stain for p-ERK (*A*) and p-S6 (*D*), thereby indicating enhanced Ras/Raf/MEK/ERK signaling (as evidenced by the presence of p-ERK) and mTOR signaling (as evidenced by the presence p-S6) in these tumors. Two or three sarcomas were evaluated for each *Kras; p16p19^{null}* category. (*B*, *C*, *E*, and *F*) Immunohistochemcial staining of commercially available tissue arrays (S02081; US Biomax) shows that human RMS tumors and leiomyosarcomas express p-ERK in 44–50% of cases (*B* and *C*) and p-S6 in 26–33% of cases (*E* and *F*). Duplicate cores were provided for each case. Images were obtained at 20× magnification.

Table S1. MFA cells in *p16p19^{null}* and wild-type C57BL6 mice

Table S1 (DOCX)

Summary of functional properties of satellite cells, Sca1$^+$ cells, CXCR4$^-$ cells, and CD45$^+$MAC1$^+$TER119$^+$ cells isolated from mouse skeletal muscle. *p16p19^{null}* muscle showed equivalent mass (1,323 ± 217 mg vs. 1,577 ± 494 mg in 25- to 48-d old mice; $P = 0.1$) and differentiation capacity among individual subpopulations of MFA cells (Fig. 1 *A* and *B* and Fig. S1 *A* and *B*). Data are presented as mean (± SD) and were obtained from evaluation of 30 *p16p19^{null}* mice (12 ♀, 18 ♂, age 22–48 d, $n = 8$ independent experiments) and 31 C57BL6 mice (all ♂ age 29–41 d, $n = 7$ independent experiments). Statistical significance was determined by Bonferroni's multiple comparison test.

Table S2. GSEA evaluating enrichment of *Kras; p16p19^{null}* sarcoma–up-regulated genes in published human sarcoma, human carcinoma, mouse sarcoma, and mouse nonsarcomatous cancer datasets

Table S2 (DOCX)

GSEA analysis at various fold-change levels showed that the *Kras; p16p19^{null}*-associated gene set is enriched significantly in several human sarcoma subtypes (including embryonal RMS, alveolar RMS, pediatric non-RMS soft-tissue sarcoma, and malignant fibrous histiocytoma) and in human pancreatic adenocarcinoma but not in human lung adenocarcinoma, human colon adenocarcinoma, or human prostate adenocarcinoma. Moreover, the *Kras; p16p19^{null}*-associated gene set is enriched significantly in mouse sarcomas (including *Kras; Tp53^{null}* mouse sarcomas with myofibroblastic differentiation and *PAX3-FKHR$^+$; TP53^{null}* mouse alveolar RMS) as well as in mouse *KrasG12(V)* lung tumors and *Kras*-infected mouse embryonic fibroblasts but not in mouse medulloblastoma and mouse mammary tumors. Thus, the *Kras; p16p19^{null}*–up-regulated gene set is enriched in sarcomas and *Ras*-driven nonsarcomatous malignancies across species. Significance is defined as an FDR q value < 0.25 and an FWER P value < 0.05.

Table S3. Kras; *p16p19*^{null} sarcoma-associated genes up-regulated in human sarcomas

Table S3 (DOCX)

List of sarcoma genes associated with Venn diagrams in Fig. S3*B*. Many of these genes have been associated previously with human malignancies (see references in table) and specifically with sarcomas (genes in bold font). By gene ontology analyses, this cluster of 144 genes can be sorted into five groups associated with the following cellular functions: cell death (58 genes), cell cycle (33 genes), cell growth and proliferation (61 genes), cellular development (46 genes), and cellular movement (44 genes). Also, 54 of these 144 genes are included in the upper quartile of genes identified by GSEA for *Ras*-transduced mammary epithelial cells (MCf10a), HEK, and human mammary epithelial cells (HMEC) cells (Fig. 3 *D–F* and Table S4) and thus are associated with *Ras* pathway activation.

Table S4. GSEA evaluating enrichment of the conserved cluster of sarcoma–up-regulated genes in oncogene-transduced human cell lines

Table S4 (DOCX)

GSEA demonstrated enrichment of the gene set identified in Fig. 3*E* in *H-Ras*–transduced HMECs, MCF10a, and HEK cells but not in HMECs transduced with Myc, BCAT, or E2F3. Significance is defined as an FDR q value < 0.25 and an FWER P value < 0.05.

Dataset S1. Microarray reference information. Reference information for microarray data, including previously published datasets and the Kras; p16p19null sarcoma dataset. The original CEL files on human RMS and non-RMS soft-tissue sarcomas are available at https://array.nci.nih.gov/caarray/project/details.action?project.experiment.public Identfier = trich-00099 (1)

Dataset S1 (XLS)

1. Davicioni E, et al. (2009) Molecular classification of rhabdomyosarcoma—genotypic and phenotypic determinants of diagnosis: A report from the Children's Oncology Group. *Am J Pathol* 174:550–564.

Dataset S2. Key for heatmap in Fig. S3*A*. Affymetrix probe identifiers denoting probes up-regulated >25-fold in *Kras; p16p19*^{null} mouse sarcomas compared with skeletal muscle were converted into gene IDs and assessed for inclusion on the hu6800, hu133a, and hu133a2 Affymetrix platforms. These gene IDs constitute the heatmap shown in Fig. S3*A*. The sequence of probe identifiers in Fig. S3*A* is listed here

Dataset S2 (XLS)

Dataset S3. Key for heatmap in Fig. S4*A*. Affymetrix probe identifiers denoting probes up-regulated >25-fold in *Kras; p16p19*^{null} mouse sarcomas compared with skeletal muscle were converted into gene IDs and assessed for inclusion on the hu6800, hu133a, and hu133a2 Affymetrix platforms. These gene IDs constitute the heatmap shown in Fig. S4*A*. The sequence of probe identifiers in Fig. S4*A* is listed here

Dataset S3 (XLS)

Dataset S4. Key for heatmap in Fig. S4*F*. Affymetrix probe identifiers denoting probes up-regulated >25-fold in *Kras; p16p19*^{null} mouse sarcomas compared with skeletal muscle were converted into gene IDs and assessed for inclusion on the hu6800, hu133a, and hu133a2 Affymetrix platforms. These gene IDs constitute the heatmap shown in Fig. S4*F*. The sequence of probe identifiers in Fig. S4*F* is listed here

Dataset S4 (XLS)